J. Am. Soc. Mass Spectrom. (2016) 27:1089–1098
DOI: 10.1007/s13361-016-1359-3

FOCUS: MASS SPECTROMETRY AS A PROBE OF HIGHER ORDER PROTEIN STRUCTURE: RESEARCH ARTICLE

Selective Covalent Chemistry via Gas-Phase Ion/ion Reactions: An Exploration of the Energy Surfaces Associated with N-Hydroxysuccinimide Ester Reagents and Primary Amines and Guanidine Groups

Jiexun Bu, Christine M. Fisher, Joshua D. Gilbert, Boone M. Prentice, Scott A. McLuckey

Department of Chemistry, Purdue University, West Lafayette, IN 47907-2084, USA

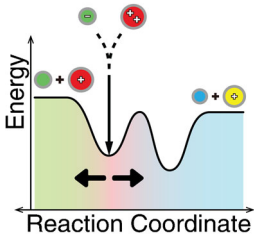

Abstract. Selective covalent bond forming reactions (referred to as covalent reactions) can occur in gas-phase ion/ion reactions and take place via the formation of a long-lived chemical complex. The gas-phase ion/ion reactivity between sulfo-*N*-hydroxysuccinimide (sulfo-NHS) ester reagent anions and peptide cations containing a primary amine or guanidine group has been examined via DFT calculations and complex dissociation rate measurements. The results reveal insights regarding the roles of the barriers of competing processes within the complex. When the covalent reaction is exothermic, two prototypical cases, determined by the nature of the energy surface, are apparent. The product partitioning between covalent reaction and simple proton transfer upon dissociation of the long-lived complex is sensitive to activation conditions when the transition state barrier for covalent reaction is relatively high (**case 1**) but is insensitive to activation conditions when the transition state barrier is relatively low (**case 2**). Covalent reaction efficiencies are very high in **case 2** scenarios, such as when the reactive site is a guanidine and the anion attachment site is a guanidinium ion. Covalent reaction efficiencies are variable, and generally low, in **case 1** scenarios, such as when an amine is the reactive site and an ammonium ion is the site of anion attachment. A relatively long slow-heating step prior to the complex dissociation step, however, can dramatically increase covalent reaction yield in **case 1** scenarios.

Keywords: Ion/ion reactions, Covalent reactivity, Gas-phase nucleophilic substitution

Received: 4 January 2016/Revised: 28 January 2016/Accepted: 30 January 2016/Published Online: 28 March 2016

Introduction

The structural information derived from a molecule of interest via tandem mass spectrometry is often highly dependent upon the type of gaseous ion (e.g., protonated molecule, radical cation, metal-cationized species, etc.) that is generated from the molecule [1]. Gas-phase polyatomic ion/ion reactions have been shown to be particularly useful for converting ions from one type to another in the gas phase. For example, they have been used to alter charge states, usually via proton transfer [2–7], invert ion polarities [8], dissociate polypeptide ions via electron transfer [9–12], exchange metal ions for protons [13], remove metal ions [14], etc. These transformations involve the transfer of one or more charged species, such as protons, electrons, and/or metal ions. Ion/ion reactions that lead to selective covalent chemistry, a form of gas-phase chemical derivatization, have also recently been reported. Examples include Schiff base chemistry between aldehydes and primary amines [15], click chemistry for coupling azides and alkynes [16], alkyl ion transfer chemistry for alkylation of anionic sites [17], etc. A reaction that is particularly useful for derivatizing ions derived from peptides and proteins involves *N*-hydroxysuccinimide (NHS) ester reagent ions because NHS esters can react with several nucleophiles often present in polypeptides. These include, for example, unprotonated primary amines [18], unprotonated guanidine groups [19], and carboxylates [20]. NHS ester-based reagents are routinely used to modify proteins in solution for various

Electronic supplementary material The online version of this article (doi:10.1007/s13361-016-1359-3) contains supplementary material, which is available to authorized users.

Correspondence to: Scott A. McLuckey; *e-mail:* mcluckey@purdue.edu

applications and have been shown to be capable for immobilization of peptides on surfaces [21]. One such application, for example, involves protein cross-linking followed by mass spectrometry [22]. The fact that similar reactions can occur in the gas phase opens up novel possibilities for the structural characterization of gas-phase ions, such as the cross-linking of gaseous protein ions [23].

Single proton or electron transfer can occur at the crossing points on the interaction surface between the entrance channel (cation and anion pair) and the exit channels (proton transfer or electron transfer products). Due to the long-range 1/r attractive potential associated with the entrance channel, small charged particle transfers can occur without the formation of a long-lived chemical complex [24]. However ion/ion reactions that result in selective covalent bond formation must proceed through an intimate chemical complex to allow for bond breaking and formation processes. Small charged particle transfer can also occur via a long-lived chemical complex and this constitutes a major side-reaction pathway. This study was motivated by the intent to gain insights into factors that affect the relative partitioning of ion/ion reactions between covalent chemistry channels and proton transfer, the most common small particle transfer process, upon breakup of the gas-phase chemical complex. We have performed calculations and experiments using relatively small model systems to gain insights into the relevant potential energy surfaces associated with NHS ester-based reagents in reactions with primary amines and guanidines. The overall approach presented here can be generalized to other specific covalent ion/ion chemistries.

Materials and Methods

N-hydroxysulfosuccinimide (sulfo-NHS), 1-ethyl-3-(3-dimethylaminopropyl)carbodiimide (EDC), and benzoic acid were purchased from Thermo Scientific (Rockford, IL, USA). The peptides KGAGGKGAGGKL, RGAGGKGAGGKL, and RGAGGRGAGGRL were custom synthesized by NeoBioLab (Cambridge, MA, USA). Methanol was purchased from Macron Chemicals (part of Avantor, Center Valley, PA, USA). Water was purified at 15 MΩ using a Barnstead nanopure infinity ultrapure water system from Thermo Fisher Scientific (Waltham, MA, USA).

Mass Spectrometry

Experiments were performed on a dual source home-built 3D ion trap mass spectrometer [25] developed for the study of ion/ion reactions as well as a Sciex QTRAP 4000, a hybrid triple quadrupole/linear ion trap mass spectrometer [26] modified for ion/ion reactions in a manner highly analogous to the modifications described for a Sciex QTRAP 2000 instrument [27]. The 3D ion trap was also modified to enable dipolar direct current (DDC) ion activation [28]. DDC is a broad-band collisional activation technique that relies on the displacement of ions from the center of the ion trap to induce rf-heating [29]. In reactions performed on the 3D ion trap, the cations were injected into the trap axially and isolated via resonance ejection and boundary instability [25]. The reagent anion population was then injected via the opposite nano-electrospray (nESI) source. The ions were stored in the 3D ion trap simultaneously for 50–200 ms to allow for ion/ion complex formation. The complex was then isolated from the unreacted precursor ions and reaction byproducts. All DDC experiments done in 3D ion trap are carried out in 1 mTorr helium buffer gas. In the modified QTRAP 4000 platform, anions and cations were sequentially injected into the instrument via alternately pulsed nESI emitters and isolated in transit through Q1 before being transferred into the q2 reaction cell [30], which has been modified to allow for mutual storage of both ion polarities. In the q2 reaction cell [27], the ions were allowed to react for 50–200 ms. Reaction products were then transferred to Q3, where they were further probed via MS^n and mass analyzed using mass-selective axial ejection (MSAE) [31].

Rate Measurements

The dissociation rates of ion/ion reaction complexes were determined from product ion spectra acquired as a function of time at various DDC amplitudes. The dissociation of the precursor ion follows pseudo-first-order reaction kinetics, as indicated in Equation 1 [32]:

$$[M]_t = e^{-k_{diss}t} \quad (1)$$

where $[M]_t$ is the molar fraction of the ion at time t, and k_{diss} is the dissociation rate of the ion. The molar fraction is calculated by dividing the abundance of the precursor peak by the sum of the abundances of the precursor and all product ions. After taking a series of the spectra at a fixed DDC amplitude as a function of activation time, a fitting of $ln([M]_t)$ vs t yields a dissociation rate. A series of experiments at various DDC values provides dissociation rate data as a function of activation energy. Similarly, if there are two competing exit pathways, as is the case in this study, the appearance rate (i.e., fragmentation rate of individual pathway) of each product can be calculated with the quations [32]:

$$[\text{PT product}]_t = \frac{k_{PT}}{k_{diss}}\left(1-e^{-k_{diss}t}\right) \quad (2)$$

and

$$[\text{Cov. product}]_t = \frac{k_{cov}}{k_{diss}}\left(1-e^{-k_{diss}t}\right) \quad (3)$$

where $[\text{PT product}]_t$ and $[\text{Cov. product}]_t$ are the molar fractions of the product ions from the competing proton transfer and covalent reactions, and k_{PT} and k_{cov} are the respective appearance rates. Since proton transfer and covalent reaction are the only two observed channels for the reaction discussed below, $k_{diss} = k_{PT} + k_{cov}$.

All DDC kinetics experiments were conducted using the same rf amplitude applied to the ring-electrode. For a pure

quadrupole field, the effective temperature to which an ion is raised under DDC conditions is dependent upon the DDC voltage/rf-amplitude ratio [29]. When significant contributions from higher order multi-pole fields are present, as is the case with the 3D ion trap used in this study, the q_z-value is also a factor [33]. The relevance for this work is that the effective temperatures of the ions under study increase slightly with the mass-to-charge ratio (*m/z*) of the precursor ion.

DFT Calculations

DFT calculations were used to characterize reaction pathways. Optimizations and zero-point corrected energies (ZPE) were calculated using the Gaussian 09 package [34] at the unrestricted B3LYP/6-311G++(d,p) level of theory. Since the model molecules are small, all structures are directly optimized in Gaussian 09. Transition states were searched using the QST3 option and confirmed with intrinsic reaction coordinate (IRC) calculations [35]. All stationary points have been subjected to frequency calculations and identified as local minima (zero imaginary frequencies) or transition states (one imaginary frequency).

Results and Discussion

Figure 1 provides a generalized energy diagram that depicts an ion/ion entrance channel for a dication and an anion, shown entering from the back of the diagram, for formation of a long-lived chemical complex, and dissociation channels from the complex with the reaction coordinate for proton transfer proceeding to the left and that for the covalent reaction proceeding to the right. This type of diagram is used here to describe gas-phase NHS chemistry. The entrance channel is governed by the electrostatic attraction between the reactant dication and the sulfo-NHS reagent anion. When the two opposite polarity ions approach one another, they can either transfer a charged particle at a crossing point on the energy hypersurface, (hopping mechanism) [36] or form an electrostatic complex. (Electron transfer is not favored with a sulfonate reagent, and thus is not discussed here.) A possible crossing point for ground state reactants and products for proton transfer is indicated by the X-marks on the diagram. Since reactions that lead to the formation of new covalent bonds (and possibly cleavage of other bonds) require more time than either proton or electron transfer, they are assumed to proceed via the complex formation pathway. All covalent ion/ion reactions studied to date are consistent with the formation of a long-lived complex. For this reason, we focus on the energy diagram of the long-lived complex. There are two major pathways observed in sulfo-NHS reactions for the break-up of the initially formed electrostatic complex. The pathway shown on the left of the diagram is proton transfer from a charge carrying site on the reactant dication to the sulfonate group on the reagent anion resulting in a neutral sulfo-NHS reagent and an unmodified +1 charge state reactant. Based on calculation data, proton transfer from the protonated amine to the sulfonate proceeds without a reverse critical energy (i.e., a very loose transition state). The other pathway, shown to the right, leads to covalent bond formation. The reactant complex may go over one or more transition state (TS) barriers to form the product complex in

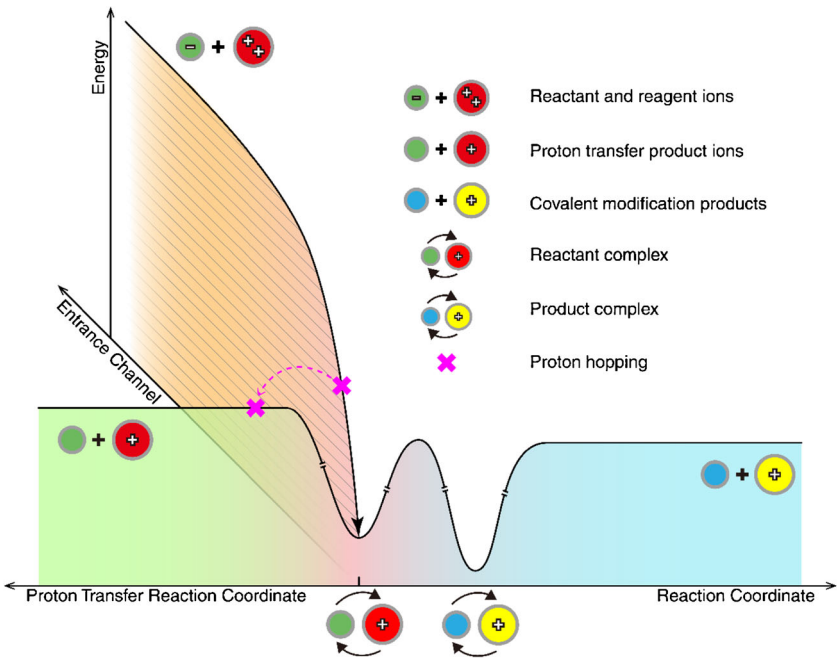

Figure 1. A generic energy diagram of a typical ion/ion reaction between a reactant dication and a reagent anion. The reactant and reagent are shown with red and green circles whereas the modified reactant and the reacted reagent are shown with yellow and blue circles. Rotating arrows show the molecule and ion are in a complex whereas the solid plus symbol shows the two species are separate. The purple x shows a crossing point where proton hopping mechanism can occur prior to long-lived complex formation

which the sulfo-NHS residue is still electrostatically bonded to the modified reactant. A rate-determining barrier is depicted in the diagram. If the sulfonate group is attached to the leaving group, as is the case when the sulfonate group is attached to the NHS group in the reagent, the product complex will reside in a relatively deep well due to the strong electrostatic interaction between the sulfonic acid and the protonated site on the cation. This product complex must then go through a proton transfer process to lose the neutral sulfo-NHS resulting in the charge-reduced modified product ion.

The barrier heights in the generalized case of Figure 1 are not defined. However, in order to generate a significant population of covalently modified product ions, the critical energy of the TS for covalent reaction and the proton transfer barrier following covalent reaction must be lower than the barrier height of the proton transfer pathway. Otherwise, upon activation, the reactant complexes will all proceed through the proton transfer pathway to the left. We also note that the TS for covalent reaction is likely to be much tighter than that for proton transfer, which places a further kinetic constraint on the observation of covalent chemistry. With these restrictions in mind, there are two generic cases that can lead to observation of covalent product. Figure 2a depicts **case 1** where the TS barrier is relatively high and it is the rate-limiting barrier in the covalent bond formation pathway. Figure 2b depicts **case 2** where the TS barrier is relatively low compared with the proton transfer barrier, and the proton transfer after modification reaction is the rate-limiting barrier for the generation of the covalently modified ion free from the leaving group.

Sulfo-NHS esters have been shown to be reactive with primary amines[18] and guanidine groups[19] in gaseous polypeptide ions (see Scheme 1). We have performed calculations of small model systems to provide realistic estimates of the key barrier heights in the energy diagrams and performed kinetics experiments with several polypeptide cations with these functional groups to provide insights into the energy diagrams that apply to these prototypical reactions. Calculations were performed on small molecule model systems because of the calculation time scales with the cube of the number of electrons [37] and because we wanted to avoid complicating effects due to interactions with other groups in the molecule that could impact the generality of the conclusions.

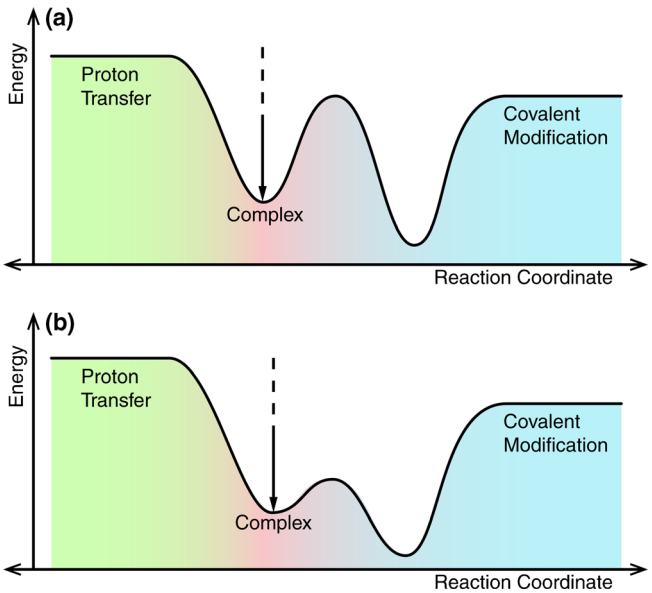

Figure 2. Two generic cases of energy diagrams that lead to at least some covalent product. **(a)** Case 1. **(b)** Case 2

Barrier Estimates of Amine Reactive Site with Ammonium Anchor Site

The key barriers for determining if a system is better represented by **case 1** or **case 2** are those associated with the barriers to proton transfer (Ⓑ→Ⓐ in the diagram of Figure 3) versus covalent reaction (Ⓑ→Ⓒ in Figure 3). For the ion/ion reactions involving NHS esters with polypeptides, both the cations and anions are bifunctional in nature in that both contain ionic sites that allow for the formation of a strong electrostatic interaction, which determines the barrier to proton transfer, and neutral reactive sites, which determine the barrier to covalent reaction. The electrostatic interaction gives the complex a sufficient lifetime for the neutral reactive sites to find one another and react and provides an upper limit to how much the complex can be heated before it dissociates. However, the ionic sites are not engaged in the covalent chemistry themselves and merely serve as spectators. In determining if a system is better represented by **case 1** or **case 2**, it is important to consider both the reactive site (amine, in this case) and the attachment site (an ammonium cation, in this case). Hence, we have used different small model systems to simulate the relevant interactions separately. Figure 3 shows a relevant energy diagram for the system of amine reactivity with ammonium attachment. The barriers Ⓑ→Ⓐ and Ⓓ→Ⓔ represent the break-up of the electrostatic interaction between the sulfonate group and a protonated amine to yield a sulfonic acid and a neutral amine (i.e., proton transfer). The Ⓑ→Ⓐ barrier was modeled via the break-up by proton transfer of the complex of ethyl sulfonate and doubly protonated *tris*(3-aminopropyl)methane (Scheme 2a R = $-NH_2$). This models the presence of two protonated amines and one neutral primary amine. The Ⓓ→Ⓔ barrier is assumed to be very similar to the Ⓑ→Ⓐ barrier in that it also involves the break-up of a sulfonate/protonated amine complex. With the electrostatic complex assigned zero energy, the proton transfer barrier was calculated to be 28 kcal/mol in zero-point corrected energy (All energies below are reported in zero-point corrected energy). The barrier Ⓑ→Ⓒ represents the energy to achieve the TS for the nucleophilic displacement of NHS by a primary amine and was modeled with methylamine and NHS-acetate (Scheme 2), see Supplementary Material for the coordinates of all of the calculated structures). With the Van der Waals complex of the reactants assigned zero energy, the barrier was calculated to be 21 kcal/mol. The subsequent IRC calculation around the transition state showed that only one TS barrier is

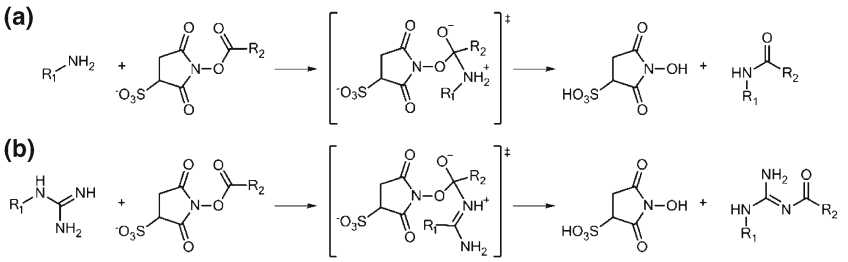

Scheme 1. Reaction scheme for the reaction between a sulfo-NHS ester reagent and **(a)** an amine and **(b)** a guanidine. The excess protons on the amine and guanidine are not shown for clarity. One of these protons is transferred to the sulfonate group upon break-up of the complex

present. Compared with the original van der Waals complex of the reactants, the product complex is 7 kcal/mol lower in energy, which indicates that at equilibrium, the NHS chemistry product is thermodynamically favored. Assuming the electrostatic interaction and the covalent interaction to be independent, it is possible to estimate the energy diagram as in Figure 3. In the case of amine reactivity/ammonium attachment, the calculations suggest that the barrier for covalent reaction is lower than that for break-up of the electrostatic interaction between a protonated amine and a sulfonate.

Rate Data for Amine Reactive Site with Ammonium Anchor Site

The doubly protonated peptide KGAGGKGAGGKL (referred to as K.K.KL) was used as a model system for amine/ammonium (i.e., amine reactive group and ammonium charge site) experiments and was reacted with singly deprotonated benzoyl sulfo-NHS ester (referred to as BSN, see Figure 4b). Figure 4 summarizes the data generated for this system. Figure 4a provides the post-ion/ion reaction spectrum, which shows residual doubly protonated peptide reactant, singly protonated peptide, likely generated via proton transfer at a crossing point, and an ion/ion complex. The complex was then isolated and subjected to DDC rate measurement experiments. Figure 4b shows a single DDC CID product ion spectrum of

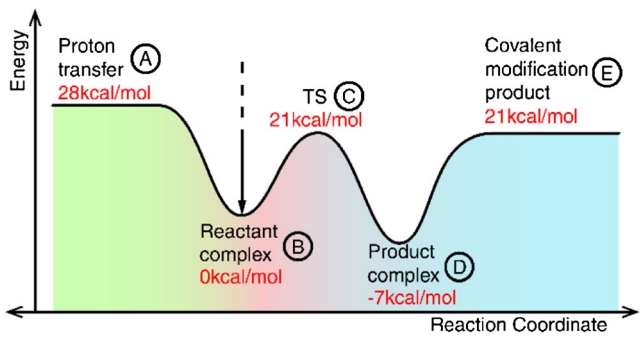

Figure 3. The PES calculated for model systems for the reaction between an amine and NHS. The barrier heights are plotted to scale. The proton transfer reaction was modeled with ethyl sulfonate and doubly protonated *tris*(3-aminopropyl)methane, whereas the nucleophilic attack reaction was modeled with methylamine and NHS-acetate

the complex, which shows a covalently modified peptide product and the singly protonated peptide from proton transfer. Figure 4c provides a summary of the kinetic data from which k_{diss} values were obtained. Figure 4d summarizes the k_{diss}, k_{PT}, and k_{cov} values derived from the K.K.KL/BSN experiments. As a control, the derivatization of K.K.KL with a benzoyl group in solution was conducted using BSN. The doubly protonated version of the resulting product (referred to as Bz-K.K.KL) was subjected to ion/ion reaction with sulfo-NHS. The resulting ion/ion complex, which is analogous to the complex between the modified peptide and deprotonated sulfo-NHS generated in the gas-phase (Ⓓ in Figure 3) was also subjected to DDC kinetics experiments (see Figure 4d).

The open black square and open triangle traces in Figure 4d show the proton transfer reaction rates and the overall covalent bond formation reaction rates, respectively, between the peptide K.K.KL and BSN. The kinetic data in Figure 4d are consistent with the DFT calculations in that both the proton transfer product and the covalent modification products are observed upon activation of the ion/ion complex. At the lowest DDC amplitude, the covalent product and proton transfer product are generated in comparable abundances while the proton transfer channel becomes more competitive as the DDC amplitude increases. This is consistent with a tighter TS for the reaction leading to the covalent product. The fact that proton transfer dominates at high DDC values for this system suggests that most of the complex ions subjected to DDC are of form Ⓑ (i.e. the complex consists of the electrostatically bound and unreacted reagent ions) in Figure 3. The proton transfer rate (looser transition state) increases faster with energy than the covalent reaction rate (tighter transition state). If most of the ion/ion complexes were of the form Ⓓ in Figure 3, the relative partitioning of the proton transfer and covalent products would be relatively insensitive to DDC amplitude (see below). In this case, the DDC is apparently required to drive the covalent chemistry within the complex.

The red circle trace in Figure 4d shows the dissociation rate of the complex generated from the solution modified peptide and deprotonated sulfo-NHS. This trace shows that loss of sulfo-NHS from the complex with a covalently modified peptide is much faster than the rate of the covalent reaction at all DDC amplitudes. This further supports the conclusion that most of the complexes initially generated by the ion/ion

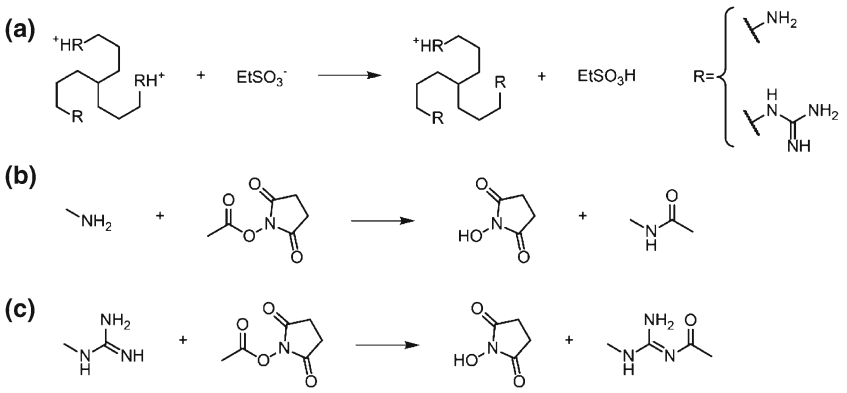

Scheme 2. The model molecules used in calculations. The proton transfer barrier is modeled by **(a)** whereas the covalent reaction is modeled by **(b)** and **(c)** for amine and guanidine, respectively

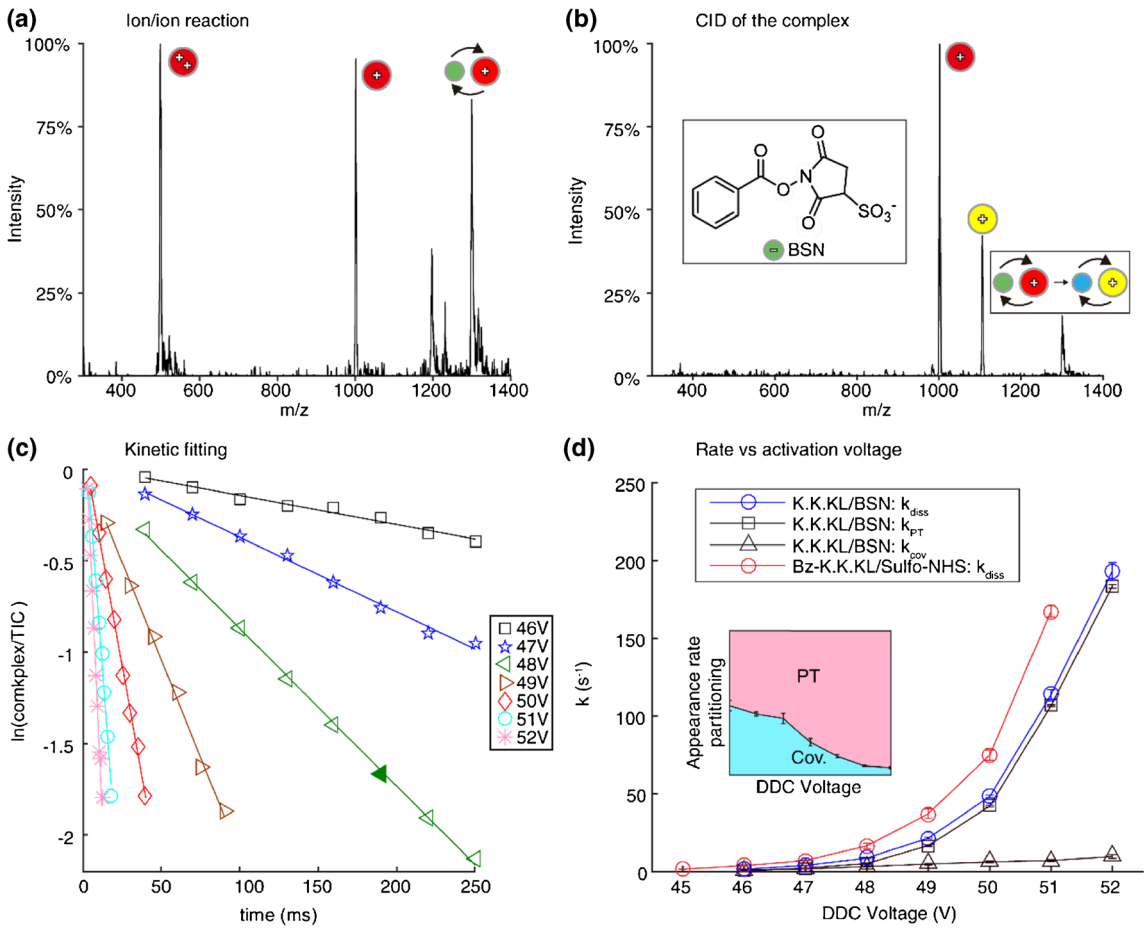

Figure 4. **(a)** Post ion/ion reaction spectrum showing residual doubly protonated KGAGGKGAGGKGAGGL (K.K.KL, *m/z* = 501), singly protonated K.K.KL (formed mostly or all by proton transfer at a crossing point, *m/z* = 1001), and the long-lived electrostatic complex (*m/z* = 1299). **(b)** The product ion spectrum obtained by DDC (48 V applied for 190 ms) of the complex. The proton transfer product appears at *m/z* = 1001 and the covalent reaction product appears at *m/z* = 1104. **(c)** The kinetic data for determining the dissociation rate of the reactant complex. The natural log of the molar fraction of the complex is plotted versus the activation time. TIC = total ion current. The different markers are different applied DDC voltages. The filled triangle represents the data of **(b). (d)** The complex dissociation rate, k_{diss}, proton transfer (PT) product appearance rate, k_{PT}, and covalent (Cov.) modification product appearance rate of reaction between K.K.KL and BSN, k_{cov}, versus DDC voltage (black trace); k_{diss} of the complex between Bz-K.K.KL and sulfo-NHS versus DDC voltage (red trace). The pink and cyan plot shows the partitioning between the covalent modification pathway rate and the proton transfer pathway, respectively. The error bars in the rate versus DDC voltage plot of **(d)** represent 1 SD of fitting error and the error bars of the insert in **(d)** are 1 SD of the rate determination

reaction are of the form Ⓑ and that reaching point Ⓒ is rate determining for the gas-phase covalent reaction process. It is also noteworthy that no reverse reaction product ([K.K.KL + H]$^+$) via Ⓓ→Ⓐ was observed in the DDC spectra of the product complex Bz-K.K.KL\Sulfo-NHS. This is also fully consistent with a tight TS associated with reaching point Ⓒ. Collectively, the kinetic data for this amine/ammonium system suggest that it falls into the **case 1** category (Figure 2a). (It is apparent that the Ⓓ→Ⓔ process for the synthesized product complex (Bz-K.K.KL with sulfo-NHS) is somewhat faster than the Ⓑ→Ⓐ process from the electrostatic complex of K.K.KL with BSN, although the shape of the rate dependencies on DDC amplitude are very similar. This suggests that there may be slightly weaker interaction between deprotonated sulfo-NHS with doubly protonated Bz-K.K.KL than between BSN and doubly protonated K.K.KL.)

Barrier Estimates of Guanidine Reactive Site with Guanidinium Anchor Site

The neutral guanidine functional group is also reactive with NHS reagents (Scheme 1b). DFT calculations analogous to those conducted for the amine/ammonium system described above were performed to estimate key barriers associated with guanidine/guanidinium reactivity. The proton transfer barrier was modeled with ethyl sulfonate and *tris*(guanidinopropyl)methane. The barrier height is 61 kcal/mol, which is significantly higher than the proton transfer barrier between the triamine and ethylsulfonate. This is attributed to the the greater proton affinity of guanidine compared with a primary amine. The TS barrier height was calculated to be 11 kcal/mol when modeled with methylguanidine and NHS-acetate, which is significantly lower than that of the amine/NHS reaction. One major transition state barrier and a barrier-free proton transfer process were observed (see Supplementary Material for geometry information). The product complex energy is 18 kcal/mol exothermic compared with the reactant complex. Here we again assume the exit channel of the product complex has a similar barrier height as the proton transfer barrier from the reactant complex due to the fact that these two processes are proton transfer from a protonated guanidine to a deprotonated sulfonate group. The results are summarized in Figure 5. In the case of guanidine/guanidinium reactivity, the TS barrier in the covalent reaction process (Ⓒ) is lower than in the amine case and the absolute barrier heights of the proton transfer pathway from both the reactant complex (Ⓑ→Ⓐ) and the product complex (Ⓓ→Ⓔ) are higher than in the amine/ammonium case. These differences suggest that the guanidine/guanidinium system would be much closer to **case 2** than the amine/ammonium system.

Rate Data for Guanidine Reactive Site with Guanidinium Anchor Site

For a model similar to that used for the amine/ammonium reactivity experiments, a peptide with the sequence RGAGGRGAGGRL (referred to as R.R.RL) was used as a guanidine/guanidinium model system to react with a benzoyl sulfo-NHS ester reagent (BSN). It has been noted that the reactivity of the N-terminus is inhibited when a basic residue is present at the N-terminus, presumably because of charge stabilization at the N-terminus due to the presence of two basic sites [12]. The majority of the reaction between BSN and R.R.RL is attributed to modification of a guanidine group. Doubly protonated R.R.RL was reacted with BSN and subjected to the same experiments summarized in Figure 4 for K.K.KL. Figure 6a shows the DDC rate data derived from the R.R.RL\BSN complex (compare with the analogous data for K.K.KL in Figure 4d). There are several notable differences between the R.R.RL and K.K.KL experiments. Perhaps the most apparent difference is that the majority of the product ions derived from activation of the complex is in the form of the covalent modification product instead of the proton transfer product. A second observation is that the proportion of covalent product is insensitive to DDC amplitude. A third observation is that the k_{diss} values for the R.R.RL/BSN complexes are consistently lower at equivalent DDC values than those for the analogous K.K.KL/BSN complexes, despite the fact that the R.R.RL/BSN complexes are elevated to slightly higher effective temperatures [33]. The latter observation is consistent with the expectation, based on the calculations, that the (Ⓑ→Ⓐ) and (Ⓓ→Ⓔ) barriers are higher for proton transfer from guanidinum to sulfonate than for proton transter from ammonium to sulfonate. Collectively, all of these data point to **case 2** as better describing the guanidine/guanidinium system than **case 1**. In this case, it is not clear that the DDC activation is necessary to drive the covalent modification.

Rate Data for Amine Reactivity with Guanidinium Charge Site

The preceding results and discussion suggest that the amine/ammonium system is best described as a **case 1** scenario and

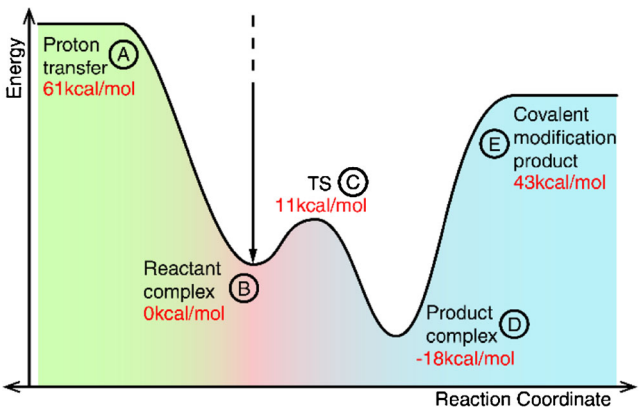

Figure 5. The PES calculated with model systems for the guanidine-NHS reaction. The barrier heights are plotted to scale. The proton transfer barrier was modeled with ethyl sulfonate and *tris*(guanidinopropyl)methane, whereas the nucleophilic attack reaction was modeled with methylguanidine and NHS-acetate

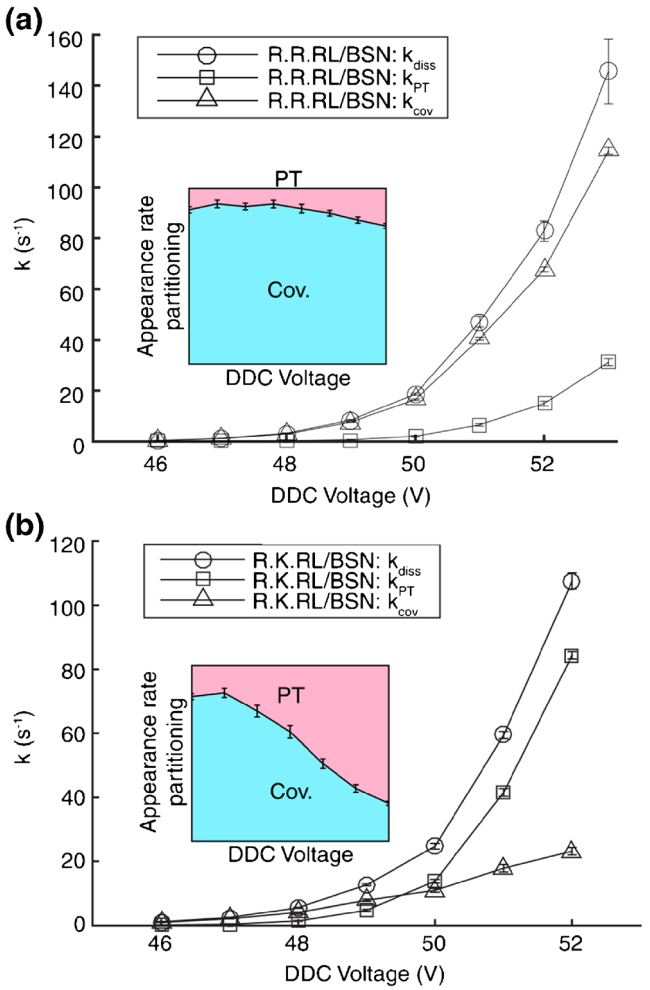

Figure 6. **(a)** The complex dissociation rate and product appearance rates of reaction between R.R.RL and BSN was plotted versus the DDC voltage applied (black traces). The pink and cyan plot shows the partitioning between the covalent modification pathway and the proton transfer pathway. The error bars in the main plot represent 1 SD of fitting error and the error bar of the insertion is calculated based on the SD of the rates. **(b)** The complex dissociation rate and product appearance rates of the reaction between R.K.RL and BSN was plotted versus the DDC voltage applied (black traces). The pink and cyan plot shows the partitioning between the covalent modification pathway rate and the proton transfer pathway. The error bars in the main plot represent 1 SD of fitting error and the error bar of the insert is calculated based on the SD of the rates

that the guanidine/guanidinium system behaves more like a **case 2** system. It is of interest to examine the behavior of amine/guanidinium and guanidine/ammonium systems. The latter scenario is experimentally difficult to realize, however, due to the fact that an excess proton will preferentially generate a guanidinium when both an amine and guanidine are present, because of the much higher proton affinity of guanidine. However, it is straightforward to generate the amine/guanidinium scenario with a peptide like RGAGGKGAGGRL (R.K.RL). In the doubly protonated peptide, the protons are most likely to be associated with the arginine residues leaving the lysine as a reactive side-chain. In this case, the DFT calculations for the (Ⓑ→Ⓐ) and (Ⓓ→Ⓔ) barriers in the guanidine/guanidinium case apply, whereas the DFT calculations for the covalent TS in the amine/ammonium case apply. This leads to an energy surface that is intermediate between the previous two cases (i.e., higher proton transfer barriers than in the amine/ammonium case and higher covalent TS barrier than in the guanidine/guanidinium case). Figure 6b summarizes the DDC activation kinetics for the R.K.RL/BSN complex. The k_{diss} values for the R.K.RL/BSN complex are similar to those of the R.R.RL/BSN complex and lower than those for the K.K.KL/BSN complex at equivalent DDC voltages, which is consistent with a guanidinium/sulfonate interaction determining the barrier to proton transfer in the R.K.RL/BSN system. At low DDC voltages, the covalent product dominates, whereas at high DDC voltages, proton transfer dominates. The behavior of the amine/guanidium sytem (i.e., R.K.RL/BSN) is intermediate to those observed for the amine/ammonium and guanidine/guanidinium sytems. The sensitivity of product partitioning to DDC amplitude suggests that the activation step is likely to be important in driving the covalent reaction. It is clear from these results that it is desirable to use low DDC amplitudes to maximize the covalent reaction in this scenario.

Covalent Modification Yield Enhancement in Case 1

In both the amine/ammonium and amine/guanidinium cases, the covalent product yield decreased with increasing DDC amplitude. In the amine/ammonium case (Figure 4), in particular, the proton transfer product was noted to be dominant even at the lowest DDC amplitudes. This behavior suggests that an equilibrium partitioning of the complexes is not achieved prior to sampling by collisional activation and that at high DDC voltages, dissociation by the proton transfer pathway is faster than rearrangement within the complex (i.e. covalent reaction). If there is an equilibrium partitioning between the initially formed electrostatic complex and the rearranged electrostatic complex generated by the covalent reaction and the latter complex is thermodynamically favored, CID should sample a population in which covalent reaction dominates. If the barrier to covalent reaction is lower than that for proton transfer, it might be possible to find conditions in which the rearrangement rate (i.e., covalent reaction) is faster than dissociation. That is, it may be possible to activate the ions sufficiently to reach the barrier for covalent reaction but not enough for appreciable dissociation via proton transfer. By subjecting the ions to the low heating step for a sufficient length of time, it might be possible to achieve a partitioning closer to equilibrium for subsequent sampling by CID or some other activation approach. We refer to the application of a low amplitude activation step prior to a more energetic activation step as "stewing". The hypothesis that a stewing step might improve covalent reaction yields in **case 1** scenarios was tested with the

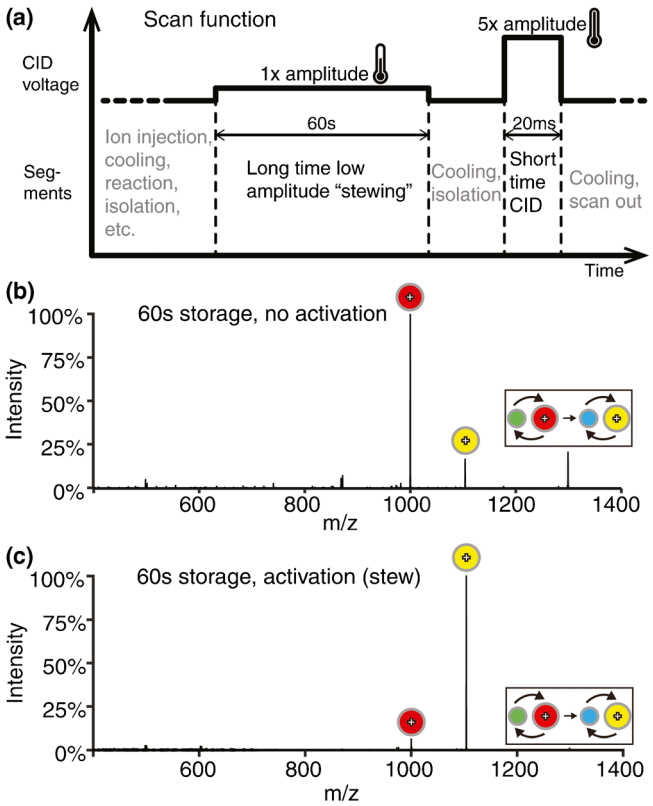

Figure 7. **(a)** Shows a simplified scan function for the "stewing" experiment. Time is not plotted to scale; **(b)** is the CID spectrum of the complex between peptide K.K.KL and BSN following a 60 s storage period without activation; **(c)** is the CID spectrum of the complex between peptide K.K.KL and BSN with a 60 s low amplitude ion activation period (i.e., a "stewing" period)

K.K.KL/NHS system, and the experiment and results are summarized in Figure 7.

Figure 7b shows a CID spectrum of the isolated complex between K.K.KL and BSN after a 60 s storage period without any supplementary ion activation. The CID amplitude was chosen so as to deplete the majority of the precursor ions within 20 ms. This corresponds to a k_{diss} in excess of 100 s^{-1}, which leads to minimal formation of the covalent reaction product. However, after applying low amplitude resonant excitation at an amplitude too low for significant fragmentation for 60 s prior to the CID segment (i.e., a "stewing" period), a dramatic increase in the proportion of covalent product is noted, as shown in Figure 7c. In this example, after the stew step another isolation was applied to remove any minor fragments in the trap. This "stewing" experiment demonstrates that most of the initially formed complex ions can be partitioned to the covalent reaction product, and the control experiment of Figure 7b (i.e., 60 s without resonance excitation) showed that the initially formed complex ions do not rearrange to the covalent reaction product at room temperature over extended periods of time.

Conclusions

This work demonstrates that the energy surfaces associated with ion/ion reactions that proceed through a long-lived chemical complex can be probed via measurement of the dissociation kinetics of the complex. The experimental results related here are consistent with calculated energy barriers based on simple models for dissociation via proton transfer of strong electrostatic interactions and for the transition states associated with nucleophilic substitution reactions leading to the loss of a sulfo-NHS group. The relative heights of the barriers for these competing processes play a major role in the extent to which exothermic covalent reactions are observed. When the TS barrier for covalent reaction is low relative to dissociation of the complex via proton transfer, high covalent reaction efficiencies are observed under all CID conditions used to dissociate the complex (**case 2**). This scenario appears to apply when guanidine is the reactive site and guanidinium is the site for electrostatic binding. When the TS barrier is relatively high, passage over the barrier within the complex can be rate-determining (**case 1**). Under these circumstances, much of the complex ion population can remain trapped as an electrostatic complex with no covalent reaction. The use of high activation amplitudes to dissociate the complex favors the faster proton transfer process resulting in the observation of very little covalent reaction. The use of low activation amplitudes allows the covalent reaction, which proceeds via a relatively tight TS, to compete with dissociation of the complex via proton transfer resulting in the observation of more of the covalent reaction product. This scenario applies to the case when an amine is the reactive site and an ammonium ion is the site of anion attachment. The case in which an amine is the reactive site and a guanidinium is the anion attachment site showed intermediate behavior. It is demonstrated that for **case 1** scenarios, a long moderate heating step for the complex prior to dissociation of the complex can lead to a dramatic increase in the yield of the covalent reaction.

Acknowledgments

This material is based upon work supported by the U.S. Department of Energy, Office of Science, Office of Basic Energy Sciences under Award Number FG02-00ER15105.

Compliance with ethical standards

Conflict of Interest The authors declare no competing financial interest.

References

1. McLuckey, S.A., Mentinova, M.: Ion/neutral, ion/electron, ion/photon, and ion/ion interactions in tandem mass spectrometry: do we need them all? Are they enough? J. Am. Soc. Mass Spectrom. **22**, 3–12 (2011)

2. Ogorzalek Loo, R.R., Winger, B.E., Smith, R.D.: Proton transfer reaction studies of multiply charged protein in a high mass-to-charge ratio quadrupole mass spectrometer. J. Am. Soc. Mass Spectrom. **5**, 1064–1071 (1994)
3. Stephenson Jr., J.L., McLuckey, S.A.: Ion/ion reactions in the gas-phase: proton transfer reactions involving multiply-charged proteins. J. Am. Chem. Soc. **118**, 7390–7397 (1996)
4. Scalf, M., Westphall, M.S., Krause, J., Kaufman, S.L., Smith, L.M.: Controlling charge states of large ions. Science **283**, 194–197 (1999)
5. Smith, L.M.: Is charge reduction in ESI really necessary? J. Am. Soc. Mass Spectrom. **19**, 629–631 (2008)
6. Coon, J.J., Ueberheide, B., Syka, J.E.P., Dryhurst, D.D., Ausio, J., Shabanowitz, J., Hunt, D.F.: Protein identification using sequential ion/ion reactions and tandem mass spectrometry. Proc. Natl. Acad. Sci. U. S. A. **102**, 9463–9468 (2005)
7. Robb, D.B., Brown, J.B., Morris, M., Blades, M.W.: Method of atmospheric pressure charge stripping for electrospray ionization mass spectrometry and its application for the analysis of large poly(ethylene glycol)s. Anal. Chem. **86**, 9644–9652 (2014)
8. He, M., McLuckey, S.A.: Two ion/ion charge inversion steps to form a doubly-protonated peptide from a singly-protonated peptide in the gas phase. J. Am. Chem. Soc. **125**, 7756–7757 (2003)
9. Syka, J.E.P., Coon, J.J., Schroeder, M.J., Shabanowitz, J., Hunt, D.F.: Peptide and protein sequence analysis by electron transfer dissociation mass spectrometry. Proc. Natl. Acad. Sci. U. S. A. **101**, 9528–9533 (2004)
10. Coon, J.J.: Collisions or electrons? Protein sequence analysis in the 21st century. Anal. Chem. **81**, 3208–3215 (2009)
11. Williams, J.P., Brown, J.M., Campuzano, I., Sadler, P.J.: Identifying drug metallation sites on peptides using electron transfer dissociation (ETD), collision induced dissociation (CID), and ion mobility mass spectrometry (IM-MS). Chem. Commun. **46**, 5458–5460 (2010)
12. Riley, N.M., Rush, M.J., Rose, C.M., Richards, A.L., Kwiecien, N.W., Bailey, D.J., Hebert, A.S., Westphall, M.S., Coon, J.J.: The negative mode proteome with activated ion negative electron transfer dissociation. Mol. Cell. Proteomics. **14**, 2644–2660 (2015)
13. Newton, K.A., McLuckey, S.A.: Gas-phase peptide/protein cationizing agent switching via ion/ion reactions. J. Am. Chem. Soc. **125**, 12404–12405 (2003)
14. Luongo, C.A., Bu, J., Burke, N.L., Gilbert, J.D., Prentice, B.M., Cummings, S., Reed, C.A., McLuckey, S.A.: Selective removal of alkali metal cations from multiply-charged ions via gas-phase ion/ion reactions using weakly coordinating anions. J. Am. Soc. Mass Spectrom. **26**, 404–414 (2015)
15. Hassell, K.M., Stutzman, J.R., McLuckey, S.A.: Gas phase bio-conjugation of peptides via ion/ion charge inversion: Schiff base formation on the conversion of cations to anions. Anal. Chem. **82**, 1594–1597 (2010)
16. Bu, J., Pilo, A.L., McLuckey, S.A.: Gas phase click chemistry via ion/ion reactions. Int. J. Mass Spectrom. **390**, 118–123 (2015)
17. Gilbert, J.D., Prentice, B.M., McLuckey, S.A.: Ion/Ion reactions with "onium" reagents: an approach for the gas-phase transfer of organic cations to multiply-charged anions. J. Am. Soc. Mass Spectrom. **29**, 818–825 (2015)
18. Mentinova, M., McLuckey, S.A.: Covalent modification of gaseous peptide ions with *N*-hydroxysuccinimide ester reagent ions. J. Am. Chem. Soc. **132**, 18248–18257 (2010)
19. McGee, W.M., Mentinova, M., McLuckey, S.A.: Gas-phase conjugation to arginine residues in polypeptide ions via *N*-hydroxysuccinimide ester-based reagent Ions. J. Am. Chem. Soc. **134**, 11412–11414 (2012)
20. Peng, Z., McGee, W.M., Bu, J., Barefoot, N.Z., McLuckey, S.A.: Gas phase reactivity of carboxylates with *N*-hydroxysuccinimide esters. J. Am. Soc. Mass Spectrom. **26**, 174–180 (2015)
21. Wang, P., Hadjar, O., Gassman, P.L., Laskin, J.: Reactive landing of peptide ions on self-assembled monolayer surfaces: an alternative approach for covalent immobilization of peptides on surfaces. Phys. Chem. Chem. Phys. **10**, 1512–1522 (2008)
22. Sinz, A.: Chemical cross-linking and mass spectrometry to map three-dimensional protein structures and protein–protein interactions. Mass Spectrom. Rev. **25**, 663–682 (2006)
23. Webb, I.K., Mentinova, M., McLuckey, S.A.: Gas-phase intramolecular protein crosslinking via ion/ion reactions: ubiquitin and a homobifunctional sulfo-NHS ester. J. Am. Soc. Mass Spectrom. **24**, 733–743 (2013)
24. Gunawardena, H.P., He, M., Chrisman, P.A., Pitteri, S.J., Hogan, J.M., Hodges, B.D.M., McLuckey, S.A.: Electron transfer versus proton transfer in gas-phase ion–ion reactions of polyprotonated peptides. J. Am. Chem. Soc. **127**, 12627–12639 (2005)
25. Wells, J.M., Chrisman, P.A., McLuckey, S.A.: Dueling electrospray: instrumentation to study ion/ion reactions of electrospray-generated cations and anions. J. Am. Soc. Mass Spectrom. **13**, 614–622 (2002)
26. Hager, J.W.: A new linear ion trap mass spectrometer. Rapid Commun. Mass Spectrom. **16**, 512–526 (2002)
27. Xia, Y., Wu, J., Londry, F.A., Hager, J.W., McLuckey, S.A.: Mutual storage mode ion/ion reactions in hybrid linear ion trap. J. Am. Soc. Mass Spectrom. **16**, 71–81 (2005)
28. Prentice, B.M., Santini, R.E., McLuckey, S.A.: Adaptation of a 3-D quadrupole ion trap for dipolar DC collisional activation. J. Am. Soc. Mass Spectrom. **22**, 1486–1492 (2011)
29. Tolmachev, A.V., Vilkov, A.N., Bogdanov, B., Păsa-Tolić, L., Masselon, C.D., Smith, R.D.: Collisional activation of ions in rf ion traps and ion guides: the effective ion temperature treatment. J. Am. Soc. Mass Spectrom. **16**, 1616–1628 (2004)
30. Xia, Y., Liang, X., McLuckey, S.A.: Pulsed dual electrospray ionization for ion/ion reactions. J. Am. Soc. Mass Spectrom. **16**, 1750–1756 (2005)
31. Londry, F.S., Hager, J.W.: Mass selective axial ion ejection from a linear quadrupole ion trap. J. Am. Soc. Mass Spectrom. **14**, 1130–1147 (2003)
32. Vékey, K.: Internal energy effects in mass spectrometry. J. Mass Spectrom. **31**, 445–463 (1996)
33. Prentice, B.M., McLuckey, S.A.: Dipolar DC collisional activation in a "stretched" 3-D ion trap: the effect of higher order fields on rf-heating. J. Am. Soc. Mass Spectrom. **23**, 736–744 (2012)
34. Frisch, M.J., Trucks, G.W., Schlegel, H.B., Scuseria, G.E., Robb, M.A., Cheeseman, J.R., Scalmani, G., Barone, V., Mennucci, B., Petersson, G.A., et al.: Gaussian 09. Gaussian, Inc., Wallingford (2009)
35. Fukui, K.: The path of chemical reactions—the IRC approach. Acc. Chem. Res. **14**, 363–368 (1981)
36. Wells, J.M., Chrisman, P.A., McLuckey, S.A.: Formation and characterization of protein–protein complexes in vacuo. J. Am. Chem. Soc. **125**, 7238–7249 (2003)
37. Cramer, C.J.: Essentials of computational chemistry: theories and models, 2nd edn. Wiley, Hoboken, NJ (2004)